Electric field tuning of excitonic fine-structure splitting in asymmetric InAs/InP nanowire quantum dot molecules

Michał Świderski* and Michał Zieliński†

Institute of Physics, Faculty of Physics, Astronomy and Informatics Nicolaus Copernicus University, 87-100 Toruń, Poland

(Received 9 October 2019; revised manuscript received 22 November 2019; published 10 December 2019)

We use an atomistic model to show that coupling between two nanowire quantum dots, forming an artificial molecule, can be used to control bright exciton splitting in these systems with external electric field and even reduce it to zero or reverse it. Importantly, strong interdot coupling allows this reduction to occur without a simultaneous detrimental reduction of excitonic optical activity, which is inherently present in weakly coupled systems. Our results indicate that nanowire quantum dot molecules could form a promising platform for quantum dot–based entanglement generation.

DOI: 10.1103/PhysRevB.100.235417

I. INTRODUCTION

A pair of coupled semiconductor quantum dots is a solid-state counterpart of a molecular system [1–7]. Artificial quantum dot molecules can be grown by using numerous approaches [8], and in different spatial configurations [9–11], whereas their spectral properties be efficiently tuned by application of external fields [4,12–17]. Numerous experimental efforts aiming at studies of quantum dot molecules have been assisted by intensive theoretical research [17–30]. Recently, nanowire quantum dot molecules [11,31,32] have gained increasing attention. In particular, the vapor-liquid-solid (VLS) growth [33] mechanism of nanowire quantum dots [34–36] offers the advantage of efficient spatial positioning [37–39] combined with high-quality optical spectra [40,41]. Moreover, nanowire quantum dots bring theoretical promise [42–46] of very low bright exciton splitting [47,48], also known as fine-structure splitting, with possible implications for quantum dot–based entanglement generation schemes [49–51]. However actual experimental measurements [52,53] of the bright exciton splitting in nanowire quantum dots very often reveal larger magnitudes of splittings, much different from theoretical predictions, likely originating from alloying effects [26,42,54,55]. Thus, similarly to self-assembled nanostructures [56–58], sample selection [51–53,59,60], or post-growth methods should likely be used for the control and the reduction of the bright exciton splitting, particularly by utilization of external electric, magnetic, and strain fields [27–29,50,61–71].

Therefore, in the following we study the effect of vertical electric field on the excitonic spectra of nanowire quantum dot molecules formed by two coupled InAs quantum dots embedded in InP nanowire. For nanowire quantum dots, the vertical electric field corresponds to a case in which the field applied along the nanowire growth direction. Here we focus on the [001] growth orientation and respectively the field is applied along [001] direction. The important case of [111]-oriented nanowire quantum dot molecules will be studied separately in our following work.

In principle, one could start by considering a symmetric quantum dot molecule built from two exactly identical quantum dots. However, such idealized quantum dot molecules were thoroughly studied in the literature [19,21–23,25,26,30], especially for Stransky-Krastanov [1,2] (self-assembled) quantum dots. Moreover, since no two quantum are ever exactly identical, here we focus on a more realistic case of a quantum dot molecule formed by two nonidentical quantum dots, namely two quantum dots of the same diameter yet different heights [72]. For that quasimolecular system we consider two interdot separations corresponding to weakly and strongly coupled quantum dots and analyze single-particle (electron and hole) spectra as well as excitonic spectra, in particular the evolution of the bright exciton splitting and its emission intensity under applied electric field. Since our analysis focuses on the symmetry properties, conclusions discussed here for nanowire quantum dot molecules could be generally be extended to Stransky-Krastanov quantum dot molecules or other quantum dot molecules of approximate C_{2v} symmetry.

II. METHODS

We study here a quantum dot molecule formed by two nonidentical InAs disk-shaped quantum dots of 2.4 nm (8 monolayers) and 1.8 nm (6 monolayers) height and 18 nm diameter, grown on a [001]-oriented InP nanowire (Fig. 1), with diameter equal to 48 nm. Dimensions considered here are consistent with our previous work [26], where we focused on the studies of role of the interdot separation. Due the VLS mechanism of nanowire quantum dots growth the assumption of nearly identical diameters is very reasonably justified, with the quantum dot diameter fixed by the dimension of the host InP nanowire and possible fluctuations in individual quantum dots heights. The much larger diameter of nanowire

*mswider@fizyka.umk.pl
†mzielin@fizyka.umk.pl

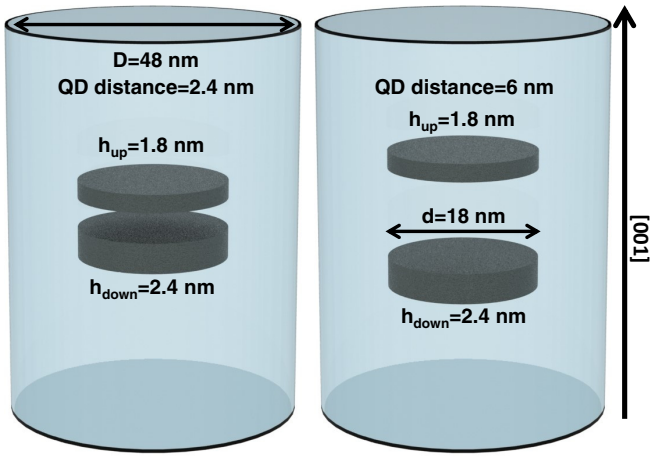

FIG. 1. Schematics of C_{2v} nanowire quantum dot molecules formed by two nonidentical disk shaped InAs quantum dots embedded in a [001]-oriented InP substrate. Right: Weakly coupled quantum dots. Left: Strongly coupled quantum dots. Electric field is applied along the nanowire growth axis. See text for more details.

corresponds to so-called clad [38] nanowire quantum dots. Finally, let us note that we consider two different interdot distances (separations), as will be discussed in detail later in the text.

The calculation starts with finding atomic positions that minimize total elastic energy. This is done by using the valence force-field method of Keating [73,74] and minimization of strain energy is performed using the conjugate gradient method [22]. In the vertical (growth) dimension we account for a section of a nanowire which is 96 nm long (thus twice the diameter equal to 48 nm, Fig. 1) and contains over 6.44 million atoms. These dimensions are sufficient for converged single-particle and many-body spectra [75] of quantum dot molecules with respect to the host nanowire section length. The valence force method is described in more detail in Refs. [76,77] and in our previous papers [22,78–80]. Next, from atomic positions, the piezoelectric potential [81–85] is calculated by accounting for both linear and quadratic contributions. Here we use piezoelectric coefficients from Ref. [83]. Then the single-particle spectra of electrons and holes are obtained with the empirical tight-binding method accounting for d orbitals and spin-orbit interaction [79,80]. The single-particle tight-binding Hamiltonian for the system of N atoms and m orbitals per atom can be written in the language of the second quantization as follows [78]:

$$\hat{H}_{\mathrm{TB}} = \sum_{i=1}^{N}\sum_{\alpha=1}^{m} E_{i\alpha} c_{i\alpha}^{+} c_{i\alpha} + \sum_{i=1}^{N}\sum_{\alpha=1,\beta=1}^{m} \lambda_{i\alpha,\beta} c_{i\alpha}^{+} c_{i\beta} + \sum_{i=1}^{N}\sum_{j=1}^{\text{near.neigh.}}\sum_{\alpha,\beta=1}^{m} t_{i\alpha,j\beta} c_{i\alpha}^{+} c_{j\beta}, \quad (1)$$

where $c_{i\alpha}^{+}$ ($c_{i\alpha}$) is the creation (annihilation) operator of a carrier on the (spin-)orbital α localized on the site i, $E_{i\alpha}$ is the corresponding on-site (diagonal) energy, and $t_{i\alpha,j\beta}$ describes the hopping (off-site and off-diagonal) of the particle between the orbitals on the four nearest-neighboring sites. i iterates over all atoms, whereas j iterates over the four nearest neighbors only. α is a composite (spin and orbital) index of the on-site orbital, whereas β is a composite index of the neighboring atom orbital. Coupling to further neighbors is thus neglected, and $\lambda_{i\alpha,\beta}$ (on-site and off-diagonal) accounts for the spin-orbit interaction following the description given by Chadi [86], which includes the contributions from atomic p orbitals. Here we use the $sp^3d^5s^*$ parametrization of Jancu [87]. The tight-binding calculation is effectively performed on a smaller domain than the valence force-field calculation [75,88]. The tight-binding domain is a cylinder with height equal to 30 nm and diameter of 24 nm, with boundary conditions treatment as described in Ref. [88]. The buffer thickness, i.e., thickness of InP material surrounding both InAs quantum dots (in other words the separation of InAs quantum dots from the computational box boundary) exceeds 8 nm in the vertical (growth) direction and is equal to 3 nm in the lateral direction. These dimensions are sufficient to obtain electron and hole spectra with sub-meV accuracy [75,88], which is consistent with our earlier findings for self-assembled quantum dots, i.e., necessity of using relatively large buffer thickness in the growth direction, corresponding to highest confinement, whereas much smaller buffers can be used in the radial direction [75]. However, the number of atoms in the tight-binding computational box still exceeds 0.5 million, and the dimensions of the tight-binding Hamiltonian exceed 10^7. The details of the $sp^3d^5s^*$ tight-binding calculation were discussed thoroughly in our earlier papers [22,78–80,89].

Finally, the excitonic spectra are calculated with the configuration interaction method. The Hamiltonian for the interacting electrons and holes can be written in second quantization as follows [1]:

$$\hat{H}_{\mathrm{ex}} = \sum_i E_i^e c_i^\dagger c_i + \sum_i E_i^h h_i^\dagger h_i + \frac{1}{2}\sum_{ijkl} V_{ijkl}^{ee} c_i^\dagger c_j^\dagger c_k c_l + \frac{1}{2}\sum_{ijkl} V_{ijkl}^{hh} h_i^\dagger h_j^\dagger h_k h_l - \sum_{ijkl} V_{ijkl}^{eh,\mathrm{dir}} c_i^\dagger h_j^\dagger h_k c_l + \sum_{ijkl} V_{ijkl}^{eh,\mathrm{exchg}} c_i^\dagger h_j^\dagger c_k h_l, \quad (2)$$

where E_i^e and E_i^h are the single-particle electron and hole energies obtained at the single-particle stage of calculations, respectively, and V_{ijkl} are Coulomb matrix elements (Coulomb direct and exchange integrals) calculated according to the procedure given in Ref. [78]. More details on Coulomb matrix element computation for tight-binding wave functions can also be found in Refs. [90,91] as well as in our recent work [92,93].

In order to account for external electric field, the electric field potential $\hat{V}$ is added to the tight-binding Hamiltonian as follows:

$$\hat{H} = \hat{H}^0 + \hat{V}, \quad (3)$$

where $\hat{H}^0$ is zero-field tight-binding Hamiltonian and $\hat{V}$ is (diagonal) field potential calculated at each atomic site. In general, such a procedure can be computationally very challenging since it demands repeating the tight-binding calculation (and also repeating following many-body computations) for each field value corresponding to different $\hat{V}$

potential landscape. Here to pinpoint excitonic resonances, we use an alternative approach [26]. In this method we perform tight-binding calculation of $\hat{H}^0$ only once and then treat $\hat{V}$ as a perturbation solved by the exact diagonalization approach. Therefore, we start with partial diagonalization of $\hat{H}^0$:

$$\hat{H}^0\left|\Psi_i^0\right\rangle = E^i\left|\Psi_i^0\right\rangle. \tag{4}$$

We find several lowest (N_{el}) electron and hole (N_{ho}) states, which we denote with lowercase indices

$$\hat{H}^0\left|\Psi_{i,\mathrm{el}}^0\right\rangle = E_{\mathrm{el}}^i\left|\Psi_{i,\mathrm{el}}^0\right\rangle \quad i = 1, N_{\mathrm{el}} \tag{5}$$

and

$$\hat{H}^0\left|\Psi_{i,\mathrm{ho}}^0\right\rangle = E_{\mathrm{ho}}^i\left|\Psi_{i,\mathrm{ho}}^0\right\rangle \quad i = 1, N_{\mathrm{ho}}. \tag{6}$$

Next, the Hamiltonian (3) in expanded in the basis of $\hat{H}^0$ eigenstates. Due the large effective single-particle gap we perform this basis expansion separately for the electron and the hole subspaces:

$$\hat{H_{ij}^{\mathrm{el}}} = \left\langle\Psi_{i,\mathrm{el}}^0\left|\hat{H}\right|\right\rangle\Psi_{j,\mathrm{el}}^0\rangle = E_{\mathrm{el}}^i\delta_{ij} + \left\langle\Psi_{i,\mathrm{el}}^0\left|\hat{V}\right|\Psi_{j,\mathrm{el}}^0\right\rangle \tag{7}$$

and

$$\hat{H_{ij}^{\mathrm{ho}}} = \left\langle\Psi_{i,\mathrm{ho}}^0\left|\hat{H}\right|\Psi_{j,\mathrm{ho}}^0\right\rangle = E_{\mathrm{ho}}^i\delta_{ij} + \left\langle\Psi_{i,\mathrm{ho}}^0\left|\hat{V}\right|\Psi_{j,\mathrm{ho}}^0\right\rangle. \tag{8}$$

Electric-field matrix elements $\langle\Psi_i^0|\hat{V}|\Psi_j^0\rangle$ are calculated from tight-binding wave functions obtained from (5) and (6). These functions are given as a linear combinations of atomic orbitals:

$$|\Psi_i\rangle = \sum_{\alpha,\vec{R}} a_{\alpha,\vec{R}}^i|\Phi_{\alpha,\vec{R}}\rangle, \tag{9}$$

where $a_{\alpha,\vec{R}}^i$ are the basis expansion coefficients in the atomic ($\vec{R}$ centered) basis $|\Phi_{\alpha,\vec{R}}\rangle$; α iterates over all atomic orbitals on a given atom, whereas $\vec{R}$ iterates over all atoms. The V matrix elements (in a unperturbed basis) are then given as:

$$\left\langle\Psi_{i,\mathrm{el}}^0\left|\hat{V}\right|\Psi_{j,\mathrm{el}}^0\right\rangle = \sum_{\alpha,\vec{R}} a_{\alpha,\vec{R}}^{i\,*} a_{\alpha,\vec{R}}^j V(\vec{R}), \tag{10}$$

where $V(\vec{R})$ is electric-field potential on atomic site $\vec{R}$ and we have utilized atomic basis orthogonality [91]. Once constructed, Hamiltonians (7) and (8) are diagonalized, leading to electron and hole states given as linear combinations of zero-field electron and hole eigenstates:

$$|\Psi_{i,\mathrm{el}}\rangle \approx \sum_{j=1,N_{\mathrm{el}}} \gamma_{j,\mathrm{el}}^i\left|\Psi_{j,\mathrm{el}}^0\right\rangle,$$

$$|\Psi_{i,\mathrm{ho}}\rangle \approx \sum_{j=1,N_{\mathrm{ho}}} \gamma_{j,\mathrm{ho}}^i\left|\Psi_{j,\mathrm{ho}}^0\right\rangle. \tag{11}$$

Once single-particle energies and states are determined, the many-body states are calculated [78]. For the exact diagonalized wave functions, Coulomb matrix elements are now given as:

$$V_{ijkl} = \sum_{a,b,c,d} \gamma_{a,i}^*\gamma_{b,j}^*\gamma_{c,k}\gamma_{d,l}V_{abcd}^0, \tag{12}$$

where V_{abcd}^0 are calculated once for the zero-field case. The dipole matrix elements [78] are recalculated accordingly and together with Coulomb matrix elements are finally utilized to compute energy and optical spectra of excitons in an electric field.

For a single quantum dot (at the stage of the configuration interaction calculation) it is typically sufficient to account for the lowest 6 (12 with spin) single-particle levels [94]. This means accounting for s, p, and d electronic shells of a single quantum dot. Here, since we deal with two coupled quantum dots forming a molecule, we chose to account for twice as large a number, i.e., the lowest 12 (24 with spin) single-particle electron and hole states in the exact diagonalization. Namely N_{el} and N_{ho} of Hamiltonians (7) and (8) are equal to 24 (with spin). This corresponds to calculation of $24^4 = 331\,776$ Coulomb matrix elements V_{abcd}^0 for zero-field cases. We checked that (for range of field values considered in this work) such basis dimensions guarantee agreement between exact diagonalization and full, nonperturbative approach to be well within a several-percentae range, for both single-particle and many-body spectra studied in this work. Apart from challenging zero-field calculations, our approach has a significant computational advantage, especially for cases like those discussed in this paper, where numerous external field values need to be calculated for the same nanostructure. However, once excitonic anticrossings are found using the perturbative approach, we additionally run full (nonperturbative) tight-binding and configuration interaction computations for several field values in vicinity's of these crossings. This is a time-consuming calculation involving over 40 field points (16 for weakly and 25 field values for strongly coupled quantum dot molecules as discussed later), and for each of these points the single-particle (tight-binding Hamiltonian) spectra needs to be found and correspondingly a new set of Coulomb matrix elements calculated, etc. Yet, this laborious procedure allows us to verify the quality of perturbative approach, and it turns out that perturbative method (provided sufficiently large zero-field basis mentioned earlier) works exceptionally well for the calculation of the bright exciton fine structure in quantum dot molecules, as shown in the Appendix.

Finally, we note that we use standard [95] convention, where the electric field $\mathbf{F}$ is given by the negative gradient of electric potential: $\mathbf{F} = -\nabla V$. Thus, the field has the opposite sign with respect to the gradient of electric potential V (voltage drop). Therefore, negative fields correspond to a potential drop in the lower quantum dot with respect to the upper quantum dot (Fig. 1). Analogously, positive fields correspond to the increase of electric potential in the lower quantum dot with respect to the upper quantum dot.

III. WEAKLY COUPLED QUANTUM DOTS

In our recent work [26] we have thoroughly studied the role of the interdot distance on nanowire quantum dot molecules of different symmetry. Based on that research we could distinguish several characteristic interdot coupling regimes, depending on quantum dots spatial separations. There are basically two asymptotic cases corresponding to very distant or very closely spaced quantum dots. In both of these situations quantum dot molecules spectra resemble single quantum dots, either practically separated from each other or nearly merged into one, larger quantum dot. Apart from

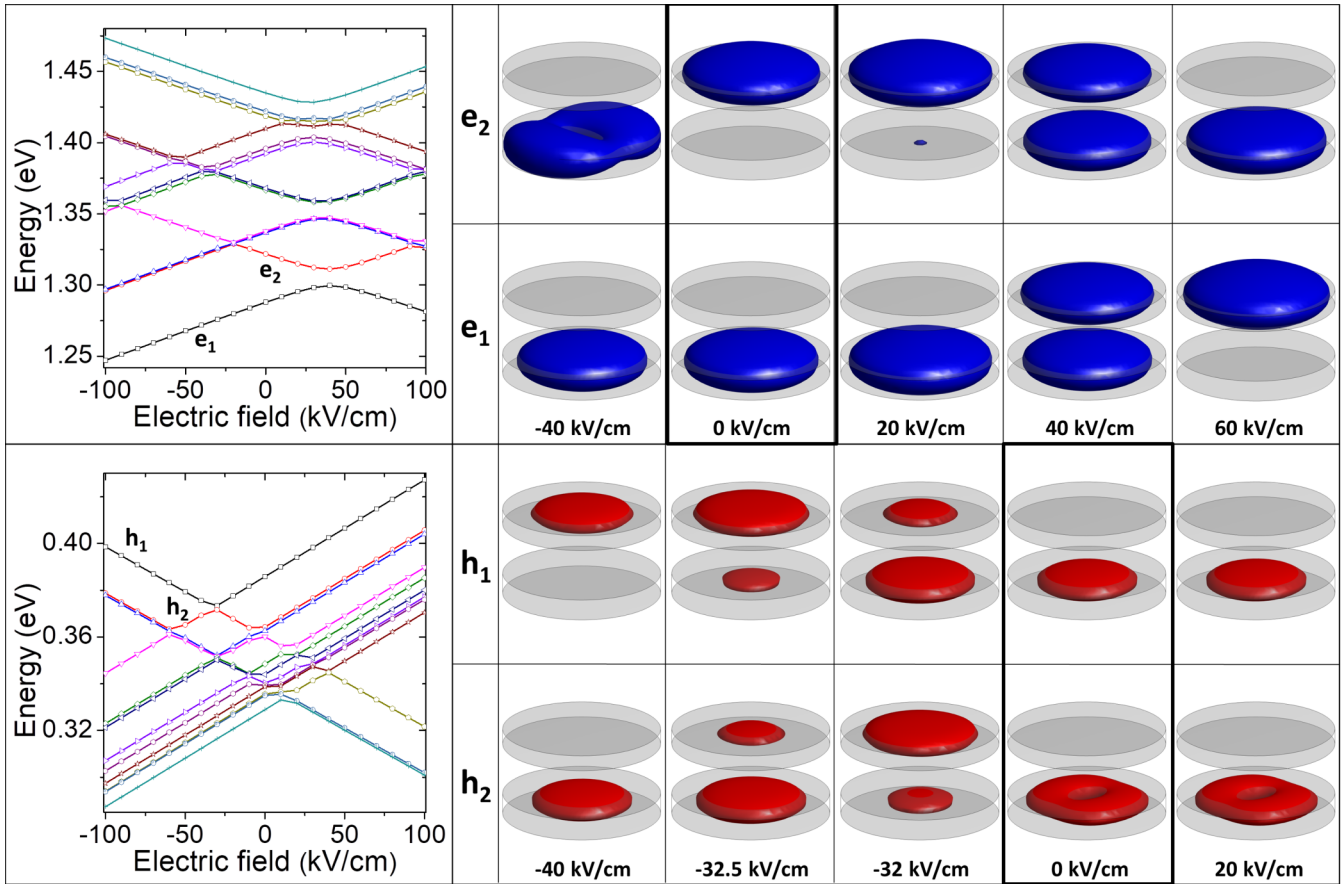

FIG. 2. Left: Single-particle electron (upper row) and hole (lower row) levels electric-field dependence for a nanowire quantum dot molecule formed by two nonidentical (see the text) weakly coupled nanowire quantum dots. The interdot distance is equal to 6 nm. Right: Corresponding single-particle electron probability density isosurfaces for selected field values for the ground electron (e_1) and hole (h_1) states, as well as the first excited electron (e_2) and hole (h_2) states. Please note thicker frames marking the zero-field cases and reverse energetic ordering of hole levels.

these extreme cases we can also consider two somewhat more interesting intermediate regimes: weakly or strongly coupled quantum dot molecules. Such division is purely conventional and could be made with a lot of freedom, yet following our earlier work [26] we will use "strong" and "weak" coupling terms as corresponding to quantum dots interdistances of approximately 2.4 nm (8 monolayers) and 6 nm (20 monolayers), respectively (Fig. 1).

Figure 2 shows single-particle electron and hole energy spectra (left) and probability densities (right) calculated for the C_{2v} nanowire quantum dot molecule formed by two nonidentical quantum dots of different heights and separated by 6 nm. Here the lower dot was arbitrarily assumed to have a larger height (Fig. 1). For [001] nanowire orientation the reverse choice, i.e., upper quantum dot being larger, would lead to an identical system from the symmetry point of view. In such case results obtained for positive field values would simply correspond to those presented here for negative field values and vice versa. On the density plot we focus on the ground and first excited electron and hole states, as those (for field values close to level crossings) are expected to form the dominant contributions to both direct and indirect excitons as discussed later. The electric-field evolution of both electron and hole levels is (to a large degree) linear under the electric field, with basically opposite trends for the electron and the hole. Trends presented on plots are, however, asymmetrical with respect to the field sign, due to inherent vertical asymmetry of the system caused by different heights of quantum dots building the asymmetric molecule. Starting from the zero-field case we note that the ground electron state is localized within the lower, larger quantum dot and is not forming a molecular-like, delocalized orbital. Similarly, the first excited electron state of the quantum dot molecule effectively origins from the upper dot and it is well localized within this dot at the zero field [96] Figure 2 shows density isosurfaces for two lowest electron and hole states only, for several different field magnitudes including the zero field. We note, however, that for the zero-field case, density isosurfaces plots of six lowest excited single-particle states were studied in detail in our earlier work [26] and can be found therein (Figs. 2 and 4). With an increasing field along the growth axis electron states can be effectively brought to a (relatively broad) resonance forming a pair of molecular ("bonding and antibonding") e_1 and e_2 states for field values at approximately 40 kV/cm, where an apparent anticrossing of electron levels is observed.

In case of a hole, both the ground and the first excited states are localized within the larger dot at zero field, resembling *s*

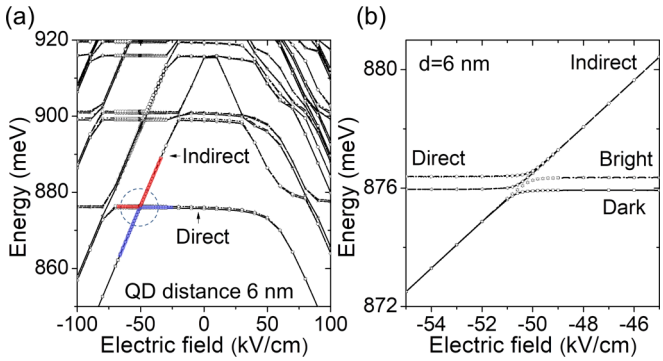

FIG. 3. (a) Exciton spectrum of weakly coupled quantum dot molecule. Energies for the high- and low-energy branch of the spectrum are plotted in dark gray (red) and light gray (blue), respectively. (b) Magnification of the excitonic spectrum close to the anticrossing. See text for details.

and p states of an individual quantum dot, respectively, and no apparent coupling to the other dot. In fact, as high as the third excited (h_4, not shown here) hole state is first to be localized predominately within the smaller quantum dot, where it origins from. The hole resonance is observed for negative field values of approximately -32 kV/cm, where the hole forms a quasimolecular state. This number is consistent with a crude estimation of approximately -43 kV/cm, which can be obtained by using $\approx$25.7 meV energy spacing between the (ground) hole state from the larger quantum dot (h_1) and the first of (excited) hole states which is localized in the smaller quantum dot at zero field (h_4) and also by taking quantum dots spacing equal to 6 nm. This simple approach overestimates the magnitude of the field needed to move the hole state from the larger dot to the smaller mostly because it does not account for spatial spread of quantum dot states; however, it provides a relatively good prediction given its simplicity.

It should be noted that for a case of electron resonance (i.e., 40 kV/cm), and formation of a delocalized electron state, the hole ground state remains localized only within the lower quantum dot. Similarly, for a field value (-32 kV/cm) leading to a formation of hole quasimolecular orbital, the ground electron state is fully localized within the single, lower quantum dot. In other words, due to differences of quantum dot heights, the formation of a quasimolecular state for one kind of charge carriers occurs when the other charge carrier is fully localized within a single dot. This will have a big impact on excitonic fine structure discussed later. Further, with field magnitudes larger than those for which single-particles resonances occur, the ground states for both carrier species are effectively separated from each other by the field and localize within opposite quantum dots.

Next, Fig. 3 shows the spectra of interacting electron and hole, forming excitonic levels. Due to opposite trends of the field evolution for individual carriers constituting the exciton, as mentioned above, the lowest excitonic state, being a "direct" exciton formed from electron and hole occupying the same quantum dot, seems to be immune to the field within about $\pm$50-kV/cm range [Fig. 3(a)]. For small field values the direct exciton practically does not vary its energy with respect to the field, manifesting its effective charge neutrality, as well as lack of the internal dipole moment and small polarizability. This is an interesting feature since based on simple arguments [4,30] one could expect such behavior only for similar, if not identical, quantum dots forming a molecule. Around about -50 kV/cm there is an apparent crossing of excitonic levels. The high-slope exciton is an "indirect" exciton formed predominately from electron and hole occupying different dots and thus of low optical activity. The flat-slope exciton is, to restate, the direct exciton dominated by many-body configurations with hole and electron localized in the same quantum dot. The indirect exciton thus has a large dipole moment due to the interdot separation and as such is susceptible to the external field contrarily to the direct exciton.

The excitonic resonance (i.e., avoided crossing in Fig. 3) is apparently related to the hole tunneling; however, due to electron-hole interaction it occurs at notably different field magnitude (-50 kV/cm) than single-particle hole resonance (-32 kV/cm). This effect can be explained by a following simple model Hamiltonian:

$$\mathbf{H} = \begin{bmatrix} E_{\mathrm{dir}X} & t \\ t & E_{\mathrm{in}X} + edF \end{bmatrix} \approx \begin{bmatrix} e_l - h_l - Je_lh_l & t \\ t & e_l - h_s - Je_lh_s - edF \end{bmatrix},$$

where $E_{\mathrm{dir}X}$ and $E_{\mathrm{in}X}$ are energies of direct and indirect excitons at zero field, given in terms of electron e and hole h single-particle energies and electron-hole Coulomb attraction J. The l and s indices denote larger and smaller quantum dot correspondingly. Here we use a convention where hole levels enter the excitonic Hamiltonian with minus signs. t is the hole tunneling coupling strength, and ed is a dipole moment of indirect exciton, with e (without a subscript) being the electron charge and d interdot distance, and F is the electric field. Assuming t is much smaller than zero-field hole states spacing, i.e., $t \ll h_s - h_l$, the excitonic levels crossing occurs for field value equal to:

$$F = (h_l - h_s + Je_lh_l - Je_lh_s)/ed, \tag{13}$$

and therefore the position of excitonic resonance depends not only on zero-field hole states energies difference but is also "renormalized" by a difference in Coulomb interaction between electron and hole states forming direct and indirect excitons. Since this difference is notable (i.e., for this case we found from atomistic calculation: $Je_lh_l \approx 24.75$ meV and $Je_lh_s \approx 12.24$ meV), accounting for the electron-hole interaction shifts the position of excitonic crossing by about -21 kV/cm, quite consistent with a result of a more accurate method (i.e., -18 kV/cm shift, from -32 to -50 kV/cm due to interactions) presented in Fig. 3.

The anticrossing of direct/indirect excitonic species has a particularly interesting effect on details of their spectra, and this is revealed in Fig. 3(b). Here the direct exciton has two branches, each corresponding to the dark and bright excitons. The lower branch is created from two dark exciton states that have negligible optical activity due to spin selection rules, similarly to single quantum dots [47]. The higher energy, bright direct exciton branch is also formed by two (optically

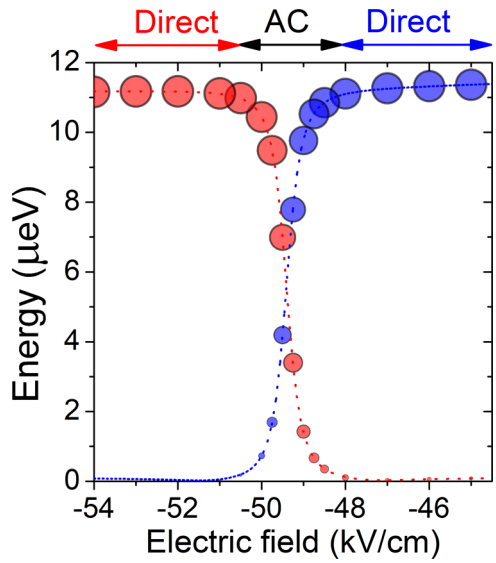

FIG. 4. Fine structure of the bright exciton spectrum in the vicinity of an anticrossing for a weakly coupled quantum dot molecule. Dark gray (red) and light gray (blue) points correspond to the calculated fine structure of the high- and low-energy exciton branches, respectively. The energies are plotted relative to the central energy of each branch for clarity. Sizes of circles correspond to oscillator strengths (emission intensities). Dashed lines are fit to atomistic results using the phenomenological model discussed in the text.

active) states. Splittings (fine structure) within bright and dark manifolds are not visible on the energy scale used in Fig. 3.

The indirect exciton is also formed by a quadruplet of two dark states, which are optically nonactive due to spin-selection rules and of two "bright" states. These spin-allowed "bright" states have, however, very weak optical activity, due to small spatial overlap of electron and hole wave functions occupying opposite quantum dots. For the same reasons, away from the anticrossing, the exchange interaction and splittings within the indirect exciton manifold are very small, practically vanishing.

To study these effects, the details of excitonic fine structure close to the anticrossing region are shown in Fig. 4. As mentioned above, for better accuracy, this calculation involves full tight-binding and configuration interaction performed for 16 different field values, with perturbative results shown for comparison in the Appendix. Here, away from the anticrossing, the fine-structure splitting is equal to 11 μeV. This splitting is present despite quantum dots forming the molecule are nonalloyed (pure InAs) disk-shaped quantum dots, and origins from low, overall C_{2v} quantum dot molecule symmetry [26,45], rather than shape-elongation of single dots [29,97,98]. Other effects, such as low-shape symmetry of individual quantum dots would likely further increase the magnitude of the bright exciton splitting [80,99]. At the anticrossing, low- and high-energy excitonic branches (direct and indirect excitons) effectively exchange magnitudes of their splitting. Despite a different material combination (InAs/InP rather than InGaAs), Fig. 4 is remarkably similar to experimental results presented in Ref. [16] [Fig. 2(c)] for self-assembled quantum dots of approximated C_{2v} symmetry. Motivated by this, we utilize here (somewhat extended) phenomenological model from that reference to fit to our atomistic calculation results. This model offers an excellent fit, which is presented in Fig. 4 as thin dashed lines. Details of the model will be discussed in the following section.

The anticrossing leads to a practically vanishing fine-structure splitting of the direct exciton. However, the drop in the fine-structure splitting is strictly followed by the decrease of its oscillator strength. A similar effect has been reported experimentally [16], as well as by calculations utilizing effective mass approximation [29] for molecules formed by elongated quantum dots. This effect is potentially detrimental for the use of weakly coupled quantum dot molecules for entanglement generation since the significant reduction of bright exciton splitting is always followed by reduction of its optical activity.

IV. STRONGLY COUPLED QUANTUM DOTS

Figure 5 shows (left) single-particle electron and hole spectra and probability densities calculated for a C_{2v} nanowire quantum dot molecule formed by two closely coupled, nonidentical quantum dots of different heights and separated by 2.4 nm. Already at the zero electric-field electron states form delocalized, molecular-like orbitals. The ground electron state appears to be formed as an bonding combination of *s*-like states from single quantum dots. The first excited state is respectively a combination of a *s*-like state from a lower dot and a *p*-like state from the upper dot. Due to small interdot distance and large interdot coupling, the antibonding combination of *s* orbitals is shifted high in energy, effectively being the third excited state (e_4) rather than first excited state (e_2) as it was in the case of weakly coupled quantum dots.

Depending on the sign, the electric field is effectively pushing the electron charge density from one dot to the another. However, due to strong spatial delocalization of electron wave function, which happens at all field values considered on the Fig. 5 (right) (i.e., -60 to 80 kV/cm), the ground electron state has a non-negligible charge density in both quantum dots.

Conversely, at zero field the ground hole state (h_1) in entirely localized in the larger (lower) quantum dot, and similarly higher hole states are well localized within their dots (either upper or lower). Therefore, at the interdot distance of 2.4 nm the hole states remain to be well localized in individual quantum dots, whereas electron states are not.

Electric field of approximately -60 kV/cm is able to bring the hole states from two quantum dots into a resonance leading to a formation of a molecular-like orbital. Notably and much differently from a weakly coupled system, at the field magnitudes where the hole ground state is molecular-like and delocalized over both quantum dots, the electron ground state preserves a nonvanishing tail and some its charge density in the smaller (upper) quantum dot.

The strong interdot coupling manifests itself as well in the excitonic spectra as shown in Fig. 6. The excitonic anticrossing occurs close to the single-particle hole resonance, yet the field magnitude at which avoided crossing appears is modified by electron-hole interactions and the anticrossing occurs at -75 kV/cm rather than at -60 kV/cm. Figure 6 reveals broad anticrossing with energy separation between

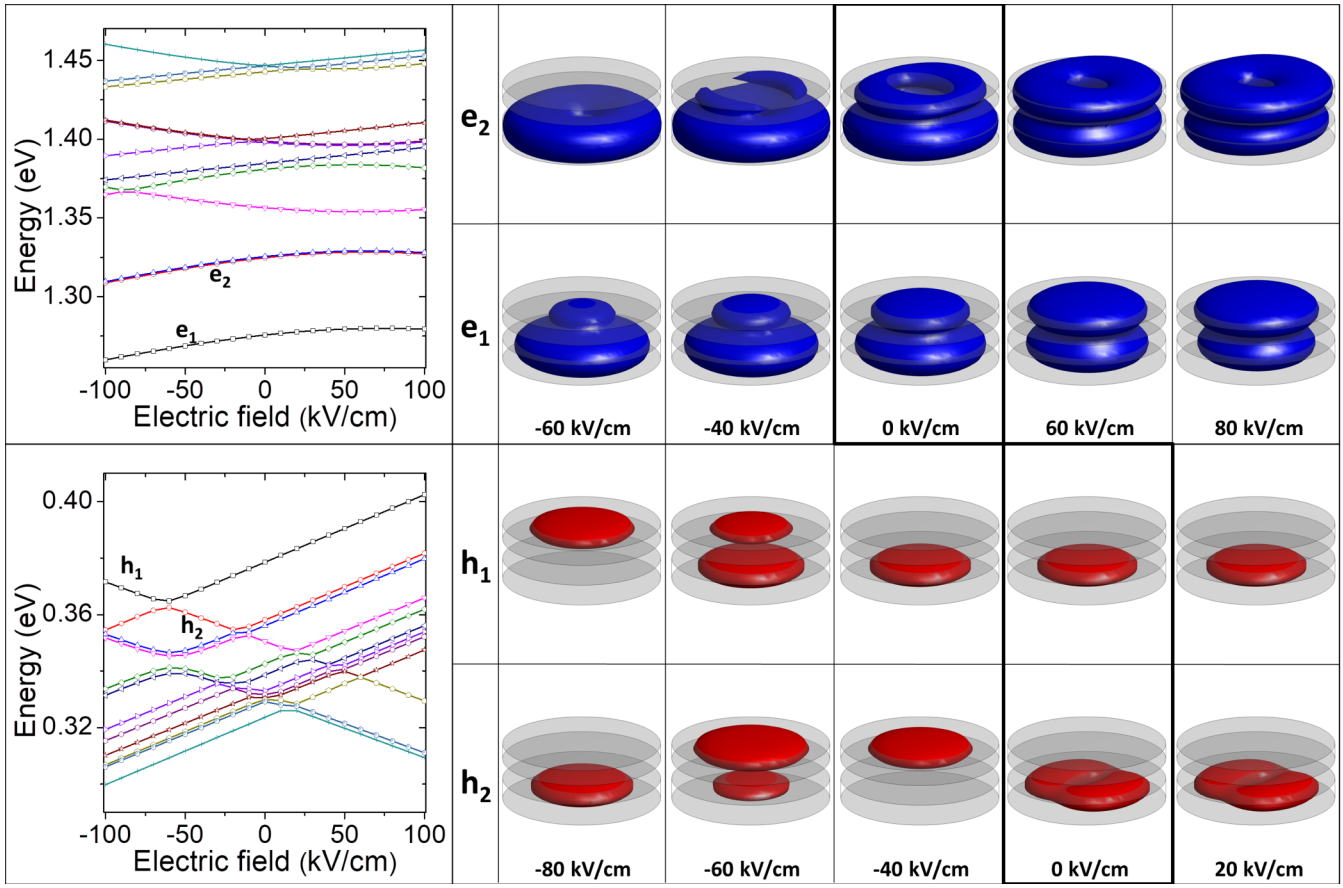

FIG. 5. Left: Single-particle electron (upper row) and hole (lower row) levels electric-field dependence for a nanowire quantum dot molecule formed by two nonidentical (see the text) strongly coupled nanowire quantum dots. The interdot distance is equal to 2.4 nm. Right: Corresponding single-particle electron probability density isosurfaces for selected field values for the ground electron (e_1) and hole (h_1) states, as well as the first excited electron (e_2) and hole (h_2) states. Please note thicker frames marking the zero-field cases and reverse ordering of hole levels.

upper and lower excitonic branches at the crossing of approximately 2 meV, about 10 times larger that in the previously discussed case of weakly coupled quantum dots. For closely spaced quantum dots, at zero field, the notion of the "direct" exciton corresponds to a lower-energy exciton constituted predominately by electron molecular-like orbital (e_1) with maximum of charge density distribution in the lower dot, as well as the hole localized in the lower dot (h_1). The indirect (the higher-energy exciton) is mostly constituted by the same electron (e_1) state, which nevertheless has a nonzero charge distribution in the upper dot and the hole localized in this upper dot (h_4). Therefore, the strong interdot coupling weakens the clear distinction between the direct/indirect exciton since the electron state contributing to both of these excitonic states is to a large degree spread over both quantum dots.

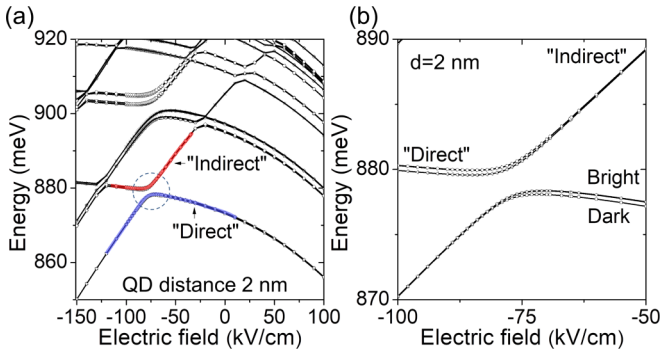

FIG. 6. (a) Exciton spectrum of strongly coupled quantum dot molecule. Energies for the high- and low-energy branch of the spectrum are plotted in dark gray (red) and light gray (blue), respectively. (b) Magnification of the excitonic spectrum close to the anticrossing. See text for details.

The strong interdot coupling and spatial spread of the electron wave function has a pronounce effect on excitonic fine-structure properties as shown in Fig. 7. Here, away from the anticrossing, the bright exciton splitting reaches a substantial value of 20 μeV. This value origins merely from the interdot coupling [26]. Thus, for the closely coupled system the magnitude of bright exciton splitting is generally significantly larger than for the weakly coupled counterpart [26]. This is therefore much different from effective mass studies of closely coupled quantum dots, as such models assume the fine-structure splitting of quantum dot molecules originating from the shape-elongation of individual quantum dots only [29].

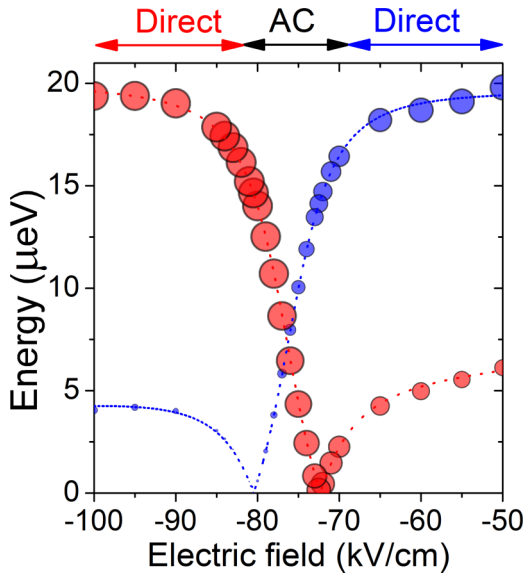

FIG. 7. Fine structure of the exciton spectrum in the vicinity of anticrossing for a strongly coupled quantum dot molecule (see the text). Dark gray (red) and light gray (blue) points correspond to the calculated fine structure of the high- and low-energy exciton branches, respectively. The energies are plotted relative to the central energy of each branch for clarity. Sizes of circles correspond to oscillator strengths (emission intensities). Dashed lines are fit to atomistic results using the phenomenological model.

Importantly, both excitonic branches undergo a transition through the zero splitting (Fig. 7). However, this happens at different field magnitude for each of excitonic species. Moreover, away from the crossing those splittings do not go asymptotically to zero but rather go to non-negligible values of several μeVs. Most importantly, whereas the lower excitonic branch loses its optical activity nearly entirely together with the reduced splitting, the higher-energy branch preserves about half of its oscillator strength even at a field value corresponding to the vanishing fine-structure splitting. Thus, much differently from the effective mass predictions [29], we show that it is possible to reduce the bright exciton splittings practically to zero, while maintaining pronounced optical activity of the exciton confined in quantum dot molecule. In other words, strongly coupled nanowire quantum dot molecules appear to be possible candidates for electron-field tuning of the bright exciton splitting and hence potentially for quantum dot molecule-based entanglement generation [7,27,28], with application of more complex electric-field configurations [100] likely needed to compensated for alloy randomness effects not discussed here.

Our results also indicate a notable difference between continuous media approximation (such as the effective mass method) and an atomistic approach. Let us note that for a single quantum dot, in a fully atomistic approach one expects to get a nonzero bright exciton splitting, even if the quantum dot has a nonelongated (cylindrical) base shape [43,45,80]. This happens because of the reduction of symmetry due to presence of the underlying crystal lattice, and this effect is simply not accounted for in a simple, effective mass modeling [97,101]. Interestingly the difference between both approaches is also present for a case of quantum dot molecules, where the bright exciton splitting can origin due to the interdot coupling as described by atomistic modeling [26], whereas it has to be "ad hoc" included [29] in an effective mass model by assuming shape elongation of individual quantum dots forming a molecule. In conclusion, in order to model details of excitonic fine structure, one must utilize methods accounting for low nanostructure symmetry [43,45,79,80,101,102] both for single and double quantum dots.

V. PHENOMENOLOGICAL MODEL

To have insight into the bright exciton splitting field evolution in the quantum dot molecule, we adopt a previously mentioned phenomenological model of Ref. [16]. In this approach, the excitonic-field evolution splitting is described by an effective Hamiltonian $\mathbf{H} = \mathbf{H}_1 + \mathbf{H}_2$, where $\mathbf{H}_1$ describes the electric-field dependence of main excitonic spectral features as follows:

$$\mathbf{H}_1 = \mathbf{I}E_X + \begin{bmatrix} -pF + \beta F^2 & 0 & t & 0 \\ 0 & -pF + \beta F^2 & 0 & t \\ t & 0 & E_h + edF + \beta_2 F^2 & 0 \\ 0 & t & 0 & E_h + edF + \beta_2 F^2 \end{bmatrix}, \tag{14}$$

where we have used the notation from Ref. [16] and I is the identity matrix, E_X is the energy of a neutral exciton confined in the larger quantum dot, and E_h is the energy required to move the hole from the larger quantum dot to the smaller quantum at zero field. t is the tunnel coupling strength, p is the permanent dipole moment along the growth axis, β is the polarizability, and F is the electric field. ed describes a much larger dipole moment of the indirect exciton, due to the separation of the electron and hole in different quantum dots, and the associated strong Stark shift is edF, where e is the electron charge, d is separation between the dots. Here we effectively treat ed, as well as E_X, E_h and all other coefficients in $\mathbf{H}_1$ as fitting parameters, while performing fit to atomistic results. Additionally, we have augmented the model with β_2 polarizability of the indirect exciton to increase the fitting subspace for better treatment of closely coupled quantum dots.

$\mathbf{H}_2$ is used here for modeling of the fine-structure component of the exciton spectrum:

$$\mathbf{H}_2 = \begin{bmatrix} 0 & \delta_{DD} & 0 & \delta_{DI} \\ \delta_{DD} & S_D - \gamma F & \delta_{DI} & 0 \\ 0 & \delta_{DI} & 0 & \delta_{II} \\ \delta_{DI} & 0 & \delta_{II} & S_I - \gamma_2 F \end{bmatrix}, \tag{15}$$

TABLE I. Parameters of H_1 obtained by fitting to atomistic results. Parameters t, E_h, and E_X are given in meV, p and ed in $10^{-1} \times$ meV kV^{-1} cm, and β and β_2 are given $10^{-4} \times$ meV kV^{-2} cm^2.

QD distance	t	p	ed	E_h	β	β_2	E_X
$d = 6$ nm	0.143	0.096	7.78	39.01	−1.81	−2.09	876.78
$d = 2.4$ nm	1.242	1.03	3.23	32.49	−3.82	−3.85	873.82

where the top-left 2×2 sub-block describes the field dependence of the direct exciton and the bottom-right 2×2 sub-block the field dependence of the indirect exciton, respectively. Bright, direct states are coupled by δ_{DD} term. Following Refs. [16,62] the fine-structure splitting of the direct exciton is effectively accounted for by two parameters, δ_{DD} and S_D, where S_D can be tuned to zero by electric field due to the $-\gamma F$ term corresponding to the difference in the permanent dipole moment between two bright states of the direct exciton. Respectively, we have added $-\gamma_2$ and δ_{II} parameters describing the coupling and the dipole moment of indirect bright exciton states. This allows us to model the strong-coupling case. Finally, the fine-structure coupling between the direct and indirect states is introduced by the δ_{DI} term.

Parameters of phenomenological Hamiltonian $\mathbf{H} = \mathbf{H}_1 + \mathbf{H}_2$ were fit to results of atomistic calculation for both weakly and strongly coupled quantum dot molecules and are shown in Tables I and II. Corresponding eigenenergies are displayed as dashed lines in Figs. 4 and 7, showing excellent fit to atomistic results.

Parameters in Table I give us an insight into the field dependence of the main excitonic features. The coupling strength t is approximately an order of magnitude larger for closely spaced quantum dots, whereas E_H and E_X are quite comparable in both cases. As expected the dipole moment of direct exciton p is practically vanishing for weakly coupled quantum dots and the field evolution is dominated by a large indirect ed dipole moment. The strongly coupled quantum dots have substantial dipole moments of both direct (p) and indirect exciton (ed), being a result of electron spatial delocalization. For closely spaced quantum dots, the indirect dipole moment ed is still (approximately 3 times) larger than the direct dipole moment p. However, since dots are closer, ed is much (about 2.4 times) smaller then for larger interdot separation. This latter ratio is in a very good agreement with the 2.5 ratio of interdot distances between weakly and strongly coupled dots, i.e., 6 nm/2.4 nm. This is thus fully consistent with initial model assumptions treating d as the interdot distance.

Finally, polarizabilities β and β_2 are about twice larger in a strong-coupling regime for both excitonic branches, reflecting again a more asymmetric/delocalized shape of the electron wave function, and more nonlinear evolution of excitonic spectra in this case (as shown earlier on Fig. 6).

As discussed above, the interdot coupling has also a pronounced effect on the excitonic fine structure. This is also visible in values of fitted parameters presented in Table II. As expected from previous discussion the zero-field parameters S_D, related to the magnitude of the direct bright exciton splitting, are generally somewhat larger for strongly coupled quantum dots, whereas δ_{DD} coupling is comparable. In fact, the bright exciton splitting (and S_D in particular) is expected to increase with decreased interdot spacing [26].

A far more pronounced difference between weakly and closely spaced quantum dots is visible in couplings between indirect exciton states (δ_{II} and S_I), which are an order of magnitude larger for 2.4-nm spaced quantum dots than for 6-nm interdot separation. In fact, the fine-structure splitting of the indirect exciton (δ_{II} and S_I) for the case of weakly coupled quantum dots could be actually neglected, without sacrificing fit quality, somewhat similar to results presented in Ref. [16]. This is much different from a case of closely spaced quantum dots, where S_I plays an essential role as will be shown in the following.

For a strongly coupled system S_I has a magnitude of approximately 8 μeV, i.e., comparable with the direct exciton $S_D \approx 13$ μeV. A reason for that being the electron forming a delocalized orbital in closely coupled quantum dots, with a substantial charge density present in the both of quantum dots. Interestingly, δ_{DI} coupling between direct and indirect dissimilar [16] spin states in practically negligible for both quantum dot separations. This is likely due to the fact that we consider a here relatively high C_{2v} symmetry with nonalloyed InAs quantum dots. Therefore δ_{DI} could in fact be neglected, and we would still get a very good quality fit.

The field dependence of H_2 is governed by the γ and γ_2 terms. For weakly coupled quantum dots γ is an order of magnitude larger than γ_2, with the latter one not being essential for this particular case. This is again similar to results of Ref. [16], where γ_2 is simply not accounted for. Consistently, we also note that we could achieve a very good quality fit for a case of weakly coupled quantum dots by imposing γ_2 equal to zero. Conversely, for the strongly coupled case γ_2 is in substantially larger than γ, and γ_2 must be accounted for.

The role S_i, δ_{ii}, and γ_2 parameters is illustrated in Fig. 8, where fit to experimental data is shown by selectively switching one of these parameters to zero. Without the indirect exciton fine structure ($S_i = 0$) the anticrossing somewhat resembles spectra of a weakly coupled quantum dot molecule, yet with none of the energy branches reaching zero fine-structure splitting. To achieve that, not only must δ_{ii} be present in the model, but also γ_2 allows for the field manipulation of the indirect exciton fine structure. From a physical point

TABLE II. Parameters of Hamiltonian H_2 obtained by fitting to atomistic results. δ's and S's are given in μeV. γ's are given in $10^{-2} \times \mu$eV kV^{-1} cm.

QD distance	δ_{DD}	δ_{DI}	δ_{II}	S_D	S_i	γ	γ_2
$d = 6$ nm	5.586	0.04	−0.035	10.58	−0.694	−18.56	1.383
$d = 2.4$ nm	4.002	−0.022	−1.106	17.759	−7.729	0.534	3.689

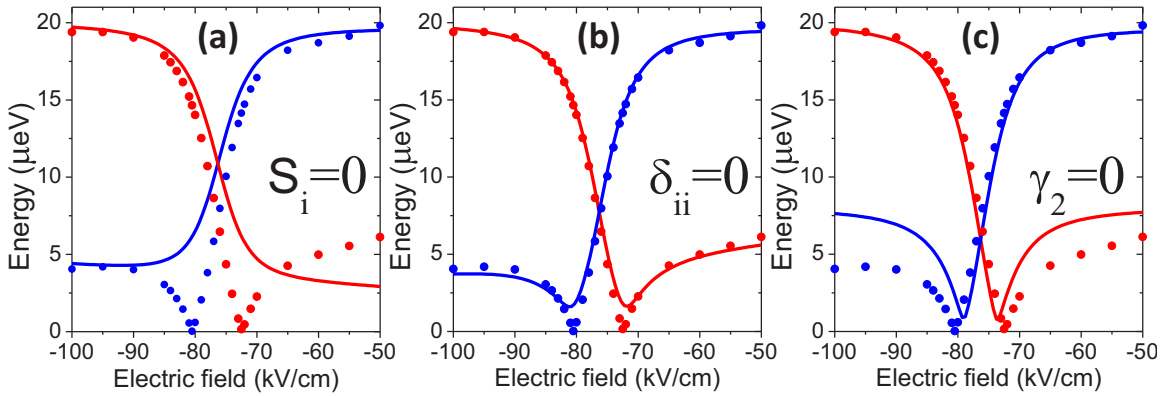

FIG. 8. Fine-structure splitting of strongly coupled molecule obtained by atomistic calculations (points) and compared with a phenomenological model with certain term set to zero (solid lines). See text for more details.

of view this describes a situation where the indirect exciton fine-structure splitting is both non-negligible ($S_i \neq 0, \delta_{ii} \neq 0$) and it has a nonvanishing dipole moment ($\gamma_2 \neq 0$). This thus gives a leverage to tune the fine-structure splitting of the strongly coupled quantum dot molecules by external electric field, allowing us to reach a vanishing magnitude of this splitting or even reverse it.

Control of the bright exciton splitting is an active field of research aiming for efficient quantum dot–based entanglement generation. In recent years, there were significant efforts related to the development of growth approaches aiming to restore high symmetry of quantum dots in hope to in turn reduce the fine-structure splitting. These efforts include the ripening [103] process, droplet epitaxy for low-strain quantum dots [104], or the VLS growth of nanowire quantum dots [34,36–39,41]. Experiments were particularly stimulated by theoretical predictions [43–45], indicating that the triangular (C_{3v}) symmetry of a nanostructure will lead to the vanishing bright exciton splitting. However, actual measurements [52,53] for nanowire quantum dots reveal bright excitons splitting varying in a broad range of values and reaching up to 18 μeV. As tailoring of morphological properties, such as size, shape, and composition and alloying [55,105], of quantum dots is typically significantly restricted by the character of epitaxial growth, numerous postgrowth methods [56–58] have been developed aiming to reduce the bright exciton splitting, most importantly by application of external fields [50,61–65,67–71]. This paper fits well into these efforts; however, we suggest using an electric field acting on quantum dot molecules rather than on single quantum dot system, and with the field applied in order to tune indirect and direct excitons, confined in nanowire quantum dot molecules, into a resonance and "mix" or "exchange" their properties. This scheme could be particularly beneficial for strongly coupled quantum dots dot where, at the anticrossing, one should expect the reduction of the bright exciton splitting without a detrimental loss of optical activity for one of excitonic branches.

VI. CONCLUSIONS

We have investigated the influence of vertical electric field on spectral properties of excitons confined in nanowire quantum dot molecules of C_{2v} symmetry. These are formed by coupled, disk-shaped InAs quantum dots of different heights embedded in host InP nanowire. We have shown that the electric field is able to tune efficiently excitonic spectra including bright exciton splitting and its emission intensity. We have considered two cases of interdot distances: weakly and strongly coupled. In both of these cases lowest hole states remain predominantly localized in the larger of two quantum dots. For the weakly coupled quantum dot molecule the electron is mostly localized in the larger dot. However, for the closely coupled system the electron ground state is delocalized over both dots, forming a quasimolecular orbital. This has a pronounced effect on the possibility of tuning the bright exciton fine structure in these nanowire quantum dot molecules. For a weakly coupled system we recover the behavior similar to that reported experimentally (for InGaAs quantum dot molecules) [16]: At the direct/indirect excitons anticrossing the decrease of the bright exciton splitting is followed by the decrease of its optical activity. However, for the closely coupled system, one of the excitonic branches goes through zero splitting, yet it does not lose its strong optical activity. As such this could predestine strongly coupled

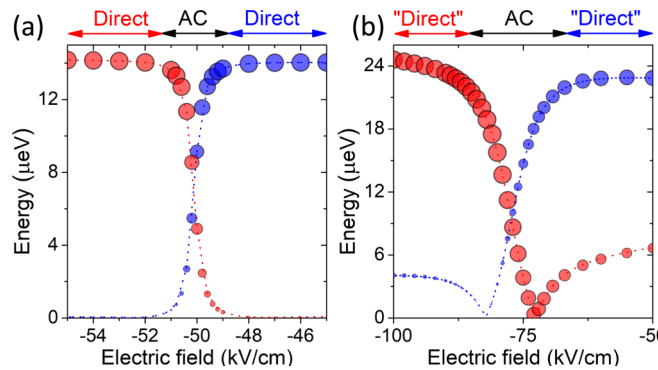

FIG. 9. Perturbative calculation of fine structure of the exciton spectrum in the vicinity of anticrossings for (a) weakly coupled and (b) strongly coupled quantum dot molecules. Dark gray (red) and light gray (blue) points correspond to the calculated fine structure of the high- and low-energy exciton branches, respectively. The energies are plotted relative to the central energy of each branch for clarity. Sizes of circles correspond to oscillator strengths (emission intensities).

quantum dot molecules for applications in the entanglement generation.

ACKNOWLEDGMENTS

M.Z. acknowledges the support from the Polish National Science Centre based on Decision No. 2018/31/B/ST3/01415.

APPENDIX: PERTURBATIVE CALCULATION OF EXCITONIC FINE STRUCTURE

The applicability of perturbative approach for calculation of excitonic fine structure is not obvious because the excitonic anticrossing occurs away from zero-field values for which single-particle spectra and Coulomb integrals are calculated. In the main part of the paper, we have presented results of excitonic fine structure obtained by a full computation; however, it turns out that the perturbative approach works remarkably well as shown on Fig. 9. Perturbative procedure generally tends to overestimates the magnitude of fine-structure splitting of direct excitons by approximately 3 to 4 μeV, as well as is predicts positions of anticrossings shifted toward more negative field values by several kV/cm. Apart from these minor points the perturbative approach performs exceptionally well and could have potential applications for other computationally demanding nanostructures.

[1] P. Michler (Ed.), *Topics in Applied Physics*, Vol. 90 (Springer, New York, 2003).

[2] D. Bimberg, M. Grundmann, and N. Ledentsov, *Quantum Dot Heterostructures* (Wiley, Chichester, 1999).

[3] M. Bayer, P. Hawrylak, K. Hinzer, S. Fafard, M. Korkusinski, Z. R. Wasilewski, O. Stern, and A. Forchel, Science **291**, 451 (2001).

[4] H. J. Krenner, M. Sabathil, E. C. Clark, A. Kress, D. Schuh, M. Bichler, G. Abstreiter, and J. J. Finley, Phys. Rev. Lett. **94**, 057402 (2005).

[5] H. J. Krenner, E. C. Clark, T. Nakaoka, M. Bichler, C. Scheurer, G. Abstreiter, and J. J. Finley, Phys. Rev. Lett. **97**, 076403 (2006).

[6] E. A. Stinaff, M. Scheibner, A. S. Bracker, I. V. Ponomarev, V. L. Korenev, M. E. Ware, M. F. Doty, T. L. Reinecke, and D. Gammon, Science **311**, 636 (2006).

[7] M. Scheibner, A. S. Bracker, D. Kim, and D. Gammon, Solid State Commun. **149**, 1427 (2009).

[8] J. Wu, Z. M. Wang *et al.*, *Quantum Dot Molecules* (Springer, Berlin, 2014).

[9] N. N. Ledentsov, V. A. Shchukin, M. Grundmann, N. Kirstaedter, J. Böhrer, O. Schmidt, D. Bimberg, V. M. Ustinov, A. Y. Egorov, A. E. Zhukov *et al.*, Phys. Rev. B **54**, 8743 (1996).

[10] O. G. Schmidt, *Lateral Alignment of Epitaxial Quantum Dots* (Springer Science & Business Media, New York, 2007).

[11] M. Khoshnegar, T. Huber, A. Predojević, D. Dalacu, M. Prilmüller, J. Lapointe, X. Wu, P. Tamarat, B. Lounis, P. Poole *et al.*, Nat. Commun. **8**, 15716 (2017).

[12] M. F. Doty, J. I. Climente, M. Korkusinski, M. Scheibner, A. S. Bracker, P. Hawrylak, and D. Gammon, Phys. Rev. Lett. **102**, 047401 (2009).

[13] M. F. Doty, J. I. Climente, A. Greilich, M. Yakes, A. S. Bracker, and D. Gammon, Phys. Rev. B **81**, 035308 (2010).

[14] M. F. Doty, M. Scheibner, I. V. Ponomarev, E. A. Stinaff, A. S. Bracker, V. L. Korenev, T. L. Reinecke, and D. Gammon, Phys. Rev. Lett. **97**, 197202 (2006).

[15] G. Ortner, M. Bayer, Y. Lyanda-Geller, T. L. Reinecke, A. Kress, J. P. Reithmaier, and A. Forchel, Phys. Rev. Lett. **94**, 157401 (2005).

[16] N. Sköld, A. Boyer de la Giroday, A. J. Bennett, I. Farrer, D. A. Ritchie, and A. J. Shields, Phys. Rev. Lett. **110**, 016804 (2013).

[17] P.-L. Ardelt, K. Gawarecki, K. Müller, A. M. Waeber, A. Bechtold, K. Oberhofer, J. M. Daniels, F. Klotz, M. Bichler, T. Kuhn *et al.*, Phys. Rev. Lett. **116**, 077401 (2016).

[18] B. W. Lovett, J. H. Reina, A. Nazir, and G. A. D. Briggs, Phys. Rev. B **68**, 205319 (2003).

[19] J. Planelles, F. Rajadell, and J. I. Climente, Phys. Rev. B **92**, 041302(R) (2015).

[20] W. Jaskolski, G. W. Bryant, J. Planelles, and M. Zieliński, Int. J. Quant. Chem. **90**, 1075 (2002).

[21] W. Jaskólski, M. Zieliński, and G. W. Bryant, Acta Phys. Pol. A **106**, 193 (2004).

[22] W. Jaskólski, M. Zieliński, G. W. Bryant, and J. Aizpurua, Phys. Rev. B **74**, 195339 (2006).

[23] G. Bester, A. Zunger, and J. Shumway, Phys. Rev. B **71**, 075325 (2005).

[24] H. S. Borges, A. M. Alcalde, and S. E. Ulloa, Phys. Rev. B **90**, 205311 (2014).

[25] M. Usman, Nanoscale **7**, 16516 (2015).

[26] M. Świderski and M. Zieliński, Phys. Rev. B **95**, 125407 (2017).

[27] M. Scheibner, S. E. Economou, A. S. Bracker, D. Gammon, and I. V. Ponomarev, JOSA B **29**, A82 (2012).

[28] C. Jennings and M. Scheibner, Phys. Rev. B **93**, 115311 (2016).

[29] H. Y. Ramírez and S.-J. Cheng, Phys. Rev. Lett. **104**, 206402 (2010).

[30] P. Schillak, Phys. Status Solidi (b) **255**, 1800231 (2018).

[31] G. Priante, F. Glas, G. Patriarche, K. Pantzas, F. Oehler, and J.-C. Harmand, Nano Lett. **16**, 1917 (2016).

[32] G. Priante, G. Patriarche, F. Oehler, F. Glas, and J.-C. Harmand, Nano Lett. **15**, 6036 (2015).

[33] R. S. Wagner and W. C. Ellis, Appl. Phys. Lett. **4**, 89 (1964).

[34] M. T. Björk, C. Thelander, A. Hansen, L. Jensen, M. Larsson, L. R. Wallenberg, and L. Samuelson, Nano Lett. **4**, 1621 (2004).

[35] L. E. Jensen, M. T. Björk, S. Jeppesen, A. I. Persson, B. J. Ohlsson, and L. Samuelson, Nano Lett. **4**, 1961 (2004).

[36] M. T. Borgström, V. Zwiller, E. Müller, and A. Imamoglu, Nano Lett. **5**, 1439 (2005).

[37] D. Dalacu, A. Kam, D. G. Austing, X. Wu, J. Lapointe, G. C. Aers, and P. J. Poole, Nanotechnology **20**, 395602 (2009).

[38] D. Dalacu, K. Mnaymneh, J. Lapointe, X. Wu, P. J. Poole, G. Bulgarini, V. Zwiller, and M. E. Reimer, Nano Lett. **12**, 5919 (2012).

[39] S. Yanase, H. Sasakura, S. Hara, and J. Motohisa, Jpn. J. Appl. Phys. **56**, 04CP04 (2017).

[40] M. E. Reimer, G. Bulgarini, N. Akopian, M. Hocevar, M. B. Bavinck, M. A. Verheijen, E. P. A. M. Bakkers, L. P. Kouwenhoven, and V. Zwiller, Nat. Commun. **3**, 737 (2012).

[41] M. Bouwes Bavinck, M. Zieliński, B. J. Witek, T. Zehender, E. P. A. M. Bakkers, and V. Zwiller, Nano Lett. **12**, 6206 (2012).

[42] R. Singh and G. Bester, Phys. Rev. Lett. **104**, 196803 (2010).

[43] R. Singh and G. Bester, Phys. Rev. Lett. **103**, 063601 (2009).

[44] M. A. Dupertuis, K. F. Karlsson, D. Y. Oberli, E. Pelucchi, A. Rudra, P. O. Holtz, and E. Kapon, Phys. Rev. Lett. **107**, 127403 (2011).

[45] K. F. Karlsson, M. A. Dupertuis, D. Y. Oberli, E. Pelucchi, A. Rudra, P. O. Holtz, and E. Kapon, Phys. Rev. B **81**, 161307(R) (2010).

[46] M. Zieliński, Phys. Rev. B **88**, 115424 (2013).

[47] M. Bayer, G. Ortner, O. Stern, A. Kuther, A. A. Gorbunov, A. Forchel, P. Hawrylak, S. Fafard, K. Hinzer, T. L. Reinecke *et al.*, Phys. Rev. B **65**, 195315 (2002).

[48] D. Gammon, E. S. Snow, B. V. Shanabrook, D. S. Katzer, and D. Park, Phys. Rev. Lett. **76**, 3005 (1996).

[49] O. Benson, C. Santori, M. Pelton, and Y. Yamamoto, Phys. Rev. Lett. **84**, 2513 (2000).

[50] R. M. Stevenson, R. J. Young, P. Atkinson, K. Cooper, D. A. Ritchie, and A. J. Shields, Nature **439**, 179 (2006).

[51] M. Prilmüller, T. Huber, M. Müller, P. Michler, G. Weihs, and A. Predojević, Phys. Rev. Lett. **121**, 110503 (2018).

[52] M. A. M. Versteegh, M. E. Reimer, K. D. Jöns, D. Dalacu, P. J. Poole, A. Gulinatti, A. Giudice, and V. Zwiller, Nat. Commun. **5**, 5298 (2014).

[53] T. Huber, A. Predojevic, M. Khoshnegar, D. Dalacu, P. J. Poole, H. Majedi, and G. Weihs, Nano Lett. **14**, 7107 (2014).

[54] M. Zieliński, K. Gołasa, M. R. Molas, M. Goryca, T. Kazimierczuk, T. Smoleński, A. Golnik, P. Kossacki, A. A. L. Nicolet, M. Potemski *et al.*, Phys. Rev. B **91**, 085303 (2015).

[55] M. Zieliński, Phys. Rev. B **100**, 045309 (2019).

[56] R. J. Young, R. M. Stevenson, A. J. Shields, P. Atkinson, K. Cooper, D. A. Ritchie, K. M. Groom, A. I. Tartakovskii, and M. S. Skolnick, Phys. Rev. B **72**, 113305 (2005).

[57] W. Langbein, P. Borri, U. Woggon, V. Stavarache, D. Reuter, and A. D. Wieck, Phys. Rev. B **69**, 161301(R) (2004).

[58] N. Akopian, N. H. Lindner, E. Poem, Y. Berlatzky, J. Avron, D. Gershoni, B. D. Gerardot, and P. M. Petroff, Phys. Rev. Lett. **96**, 130501 (2006).

[59] R. Hafenbrak, S. Ulrich, P. Michler, L. Wang, A. Rastelli, and O. Schmidt, New J. Phys. **9**, 315 (2007).

[60] F. Olbrich, J. Höschele, M. Müller, J. Kettler, S. Luca Portalupi, M. Paul, M. Jetter, and P. Michler, Appl. Phys. Lett. **111**, 133106 (2017).

[61] K. Kowalik, O. Krebs, A. Lemaitre, S. Laurent, P. Senellart, P. Voisin, and J. Gaj, Appl. Phys. Lett. **86**, 041907 (2005).

[62] A. Bennett, M. Pooley, R. Stevenson, M. Ward, R. Patel, A. B. de La Giroday, N. Sköld, I. Farrer, C. Nicoll, D. Ritchie *et al.*, Nat. Phys. **6**, 947 (2010).

[63] R. M. Stevenson, R. J. Young, P. See, D. G. Gevaux, K. Cooper, P. Atkinson, I. Farrer, D. A. Ritchie, and A. J. Shields, Phys. Rev. B **73**, 033306 (2006).

[64] B. Gerardot, S. Seidl, P. Dalgarno, R. J. Warburton, D. Granados, J. Garcia, K. Kowalik, O. Krebs, K. Karrai, A. Badolato *et al.*, Appl. Phys. Lett. **90**, 041101 (2007).

[65] S. Seidl, M. Kroner, A. Högele, K. Karrai, R. J. Warburton, A. Badolato, and P. M. Petroff, Appl. Phys. Lett. **88**, 203113 (2006).

[66] S. Marcet, K. Ohtani, and H. Ohno, Appl. Phys. Lett. **96**, 101117 (2010).

[67] J. D. Plumhof, V. Křápek, F. Ding, K. D. Jöns, R. Hafenbrak, P. Klenovský, A. Herklotz, K. Dörr, P. Michler, A. Rastelli, and O. G. Schmidt, Phys. Rev. B **83**, 121302(R) (2011).

[68] F. Ding, R. Singh, J. D. Plumhof, T. Zander, V. Křápek, Y. H. Chen, M. Benyoucef, V. Zwiller, K. Dörr, G. Bester *et al.*, Phys. Rev. Lett. **104**, 067405 (2010).

[69] J. Wang, M. Gong, G.-C. Guo, and L. He, Appl. Phys. Lett. **101**, 063114 (2012).

[70] R. Trotta, E. Zallo, C. Ortix, P. Atkinson, J. D. Plumhof, J. Van den Brink, A. Rastelli, and O. G. Schmidt, Phys. Rev. Lett. **109**, 147401 (2012).

[71] R. Trotta, J. S. Wildmann, E. Zallo, O. G. Schmidt, and A. Rastelli, Nano Lett. **14**, 3439 (2014).

[72] For [001] growth, in the idealized case of two disk-shaped nanowire quantum dots with exactly the same dimensions, compositions, and common rotational axis the overall symmetry would be D_{2d} with zero bright exciton splitting by virtue of symmetry.

[73] P. N. Keating, Phys. Rev. **145**, 637 (1966).

[74] R. M. Martin, Phys. Rev. B **1**, 4005 (1970).

[75] M. Zieliński, Acta Phys. Pol. A **122**, 312 (2012).

[76] C. Pryor, J. Kim, L. W. Wang, A. J. Williamson, and A. Zunger, J. Appl. Phys. **83**, 2548 (1998).

[77] T. Saito and Y. Arakawa, Physica E **15**, 169 (2002).

[78] M. Zieliński, M. Korkusinski, and P. Hawrylak, Phys. Rev. B **81**, 085301 (2010).

[79] M. Zieliński, Phys. Rev. B **86**, 115424 (2012).

[80] M. Zieliński, J. Phys.: Condens. Matter **25**, 465301 (2013).

[81] G. Bester, X. Wu, D. Vanderbilt, and A. Zunger, Phys. Rev. Lett. **96**, 187602 (2006).

[82] G. Bester, A. Zunger, X. Wu, and D. Vanderbilt, Phys. Rev. B **74**, 081305(R) (2006).

[83] A. Beya-Wakata, P.-Y. Prodhomme, and G. Bester, Phys. Rev. B **84**, 195207 (2011).

[84] G. Tse, J. Pal, U. Monteverde, R. Garg, V. Haxha, M. Migliorato, and S. Tomić, J. Appl. Phys. **114**, 073515 (2013).

[85] M. A. Caro, S. Schulz, and E. P. O'Reilly, Phys. Rev. B **91**, 075203 (2015).

[86] D. J. Chadi, Phys. Rev. B **16**, 790 (1977).

[87] J.-M. Jancu, R. Scholz, F. Beltram, and F. Bassani, Phys. Rev. B **57**, 6493 (1998).

[88] S. Lee, F. Oyafuso, P. von Allmen, and G. Klimeck, Phys. Rev. B **69**, 045316 (2004).

[89] J. G. Díaz, G. W. Bryant, W. Jaskólski, and M. Zieliński, Phys. Rev. B **75**, 245433 (2007).

[90] S. Lee, L. Jönsson, J. W. Wilkins, G. W. Bryant, and G. Klimeck, Phys. Rev. B **63**, 195318 (2001).

[91] S. Schulz, S. Schumacher, and G. Czycholl, Phys. Rev. B **73**, 245327 (2006).
[92] P. T. Różański and M. Zieliński, Phys. Rev. B **94**, 045440 (2016).
[93] P. T. Różański and M. Zieliński, Comput. Phys. Commun. **238**, 254 (2019).
[94] M. Zieliński, Phys. Rev. B **99**, 205402 (2019).
[95] E. M. Purcell, E. M. Purcell, E. M. Purcell, E.-U. Physicien, and E. M. Purcell, *Electricity and Magnetism*, Vol. 2 (McGraw–Hill, New York, 1965).
[96] Figure 2 shows density isosurfaces for two lowest electron and hole states only, for several different field magnitudes including the zero field. We note, however, that for the zero-field case, density isosurfaces plots of the six lowest excited single-particle states were studied in detail in our earlier work [26] and can be found therein (Figs. 2 and 4).
[97] T. Takagahara, Phys. Rev. B **62**, 16840 (2000).
[98] E. Kadantsev and P. Hawrylak, Phys. Rev. B **81**, 045311 (2010).
[99] M. Zieliński, Y. Don, and D. Gershoni, Phys. Rev. B **91**, 085403 (2015).
[100] M. Zeeshan, N. Sherlekar, A. Ahmadi, R. L. Williams, and M. E. Reimer, Phys. Rev. Lett. **122**, 227401 (2019).
[101] O. Marquardt, S. Schulz, C. Freysoldt, S. Boeck, T. Hickel, E. P. O'Reilly, and J. Neugebauer, Opt. Quantum Electron. **44**, 183 (2011).
[102] S. Tomić and N. Vukmirović, J. Appl. Phys. **110**, 053710 (2011).
[103] A. Kors, J. P. Reithmaier, and M. Benyoucef, Appl. Phys. Lett. **112**, 172102 (2018).
[104] M. Abbarchi, T. Kuroda, T. Mano, and K. Sakoda, J. Phys.: Conf. Ser. **245**, 012049 (2010).
[105] P. Mrowiński, M. Zieliński, M. Świderski, J. Misiewicz, A. Somers, J. P. Reithmaier, S. Höfling, and G. Sęk, Phys. Rev. B **94**, 115434 (2016).